Stable wüstite, FeO, nano particles, manufacturing and magnetic properties

Karl Olaf Christensen & Jari í Hjøllum

May 1, 2001

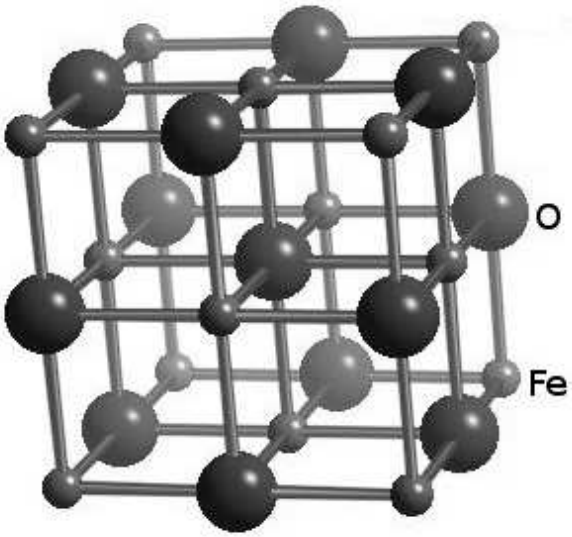

Abstract

In this report it is investigated if it is possible to produce iron oxides using sputtering with a hollow cathode cluster source using a argon-oxygen gas mixture. Mössbauer spectroscopy is used for investigating the produced iron oxides. The magnetic theory of microscopic particles is explored and used in explaining the stabilisation of wüstite nanoparticles.

Bach. Sc. in Physics
University of Copenhagen
Supervisors: Luise Theil Kuhn & Morten Bo Madsen, Ørsted laboratory
January-May 2001

Contents

1 Preface

This report appears in partial fulfilment of the requirement for the B. Sc. degree at the University of Copenhagen, Ørsted Laboratory January-May 2001. We have contributed equally to the experimental work and the report.

2 Acknowledgements

We would like to thank our supervisors Luise Theil Kuhn and Morten Bo Madsen for their good counselling during the experimental and writing process. A thank to Jan Brinchmann Christensen for taking the time to help us rig the needed apparatus. Malte Olsen deserves a thanks for helping with setting up the Mössbauer apparatus when we were in need of it. Walter Goethz has provided us with needed essential data for with we thank him. Tórdur Kruse Mørkøre has been a great help during the writing of the report. Finally we would like to thank friends and girlfriends for their patience and constant encouragement.

3 Introduction

The study of iron oxides is a very large field in modern solid state physics. Iron oxides have a wide range of application in technology, for instance in magnetic storage media, catalysator, biology etc. There is also a great interest in iron oxides in science, both in fundamental research and applicable research. For instance iron oxides are used in the investigation of the planet Mars.

The Martian surface dust is highly oxidised, and contains 13 % Fe by weight [15]. From spectroscopy it is known that the Fe is present as Fe^{3+}. More than 99 % of the Fe in the Martian surface rocks occurs as Fe^{2+}. It is certain that a oxidisation has occurred, however it is not known how. This is not the place to discuss in detail all the pathways of oxidisation i.e. the pathway from Fe^{2+} to Fe^{3+}. We limit ourselves to the following remarks on two possible pathways of the oxidisation of the surface of Mars.

The first major pathway involves the action of abundant liquid water [11]. The Fe^{2+}-ions of the rocks are released into a solution. Fe^{2+} is soluble in water. In an oxidising environment the $Fe^{2+}{}_{(aq)}$ solution is oxidised to Fe^{3+} which is insoluble in water. Therefore precipitation of iron oxides and/or hydroxides occurs. Which mineral is precipitated depends on several of the properties of the solution, and these processes are not fully understood. If the abundance of oxygen is low the oxidisation of the dissolved Fe^{2+} is slow and magnetite (Fe_3O_4) and maghemite (γ-Fe_2O_3) form. If oxygen is abundant the oxidisation of Fe^{2+} is swift and goethite (α-FeOOH) and hematite (α-Fe_2O_3) form. The formed precipitates will be iron oxides and/or hydroxides of high purity [11].

The iron oxides magnetite (Fe_3O_4) and maghemite (γ-Fe_2O_3) are strongly magnetic, and hematite (α-Fe_2O_3) and goethite (α-FeOOH) are less magnetic. Thus slow oxidisation of Fe^{2+} results in strongly magnetic minerals, whereas swift oxidisation results in less magnetic minerals.

The second pathway, is that water is involved but **not** as liquid water. Water sublimates from permafrost in the Martian surface. The water in the atmosphere is split by ultraviolet light. The hydrogen disappears and oxidative power in the form of O^- and O_2 is left on the surface of Mars[1]. Might the rocks on Mars been oxidised via gas-solid reactions, without the presence of liquid water?

However the rocks on Mars have been oxidised, it is known that a few percent of Fe^{3+} is present in an ordered magnetic phase (ferrimagnetic phase). The results of the "Magnetic Properties Experiments on Mars Pathfinder" [11][20] have shown that the mineral maghemite (γ-Fe_2O_3) is the most probable cause of the observed magnetic properties of the airborne dust on the Martian surface. However these properties are different from the properties observed in pure maghemite on earth.

[1] The Martian atmosphere contains 0.13 % O_2.

The results from Mars strongly indicate that the small dust particles on Mars are composed of several micro-crystalline phases. However there may exist another possibility, based on recent studies. These results indicate that the magnetic properties of the iron oxides hematite (α-Fe_2O_3) and maghemite, (γ-Fe_2O_3), approach each other for very small (nano-sized) particles.

The original purpose of this project was to investigate whether it is possible via sputtering (using the hollow cathode cluster source) and controlled oxidisation to manufacture nano-particle iron oxides, which are so small, that it is difficult to determine whether it is maghemite or hematite.

We were not able to produce either maghemite or hematite, but instead we were able to produce particles consisting of stable wüstite. Wüstite is normally metastable at room temperature [27].

Therefore the primary purpose of this project has been changed to manufacture wüstite, investigate the magnetic properties of it, and explain why it is stable.

We will try to set the experimental results in relation to the oxidisation of iron via gas-solid reactions. We will discuss if our results can be used to indicate whether water has been present as liquid on Mars.

The scope of this project is, in our opinion, too large for a bachelor project. It consists of two major areas: Sputtering and Mössbauer spectroscopy. It has been difficult to get the time to get acquainted with the hollow cathode cluster source used for sputtering, produce the samples, learn the Mössbauer theory, make measurements, analyse and write the project, all within the time limit. The most time consuming part of the project was to manufacture the samples. An estimate of the time used in the sputtering lab is more than 200 hours. However we have to the best of our ability tried, and the result is hereby presented to the reader.

Karl Olaf Christensen
190976-1537

Jari í Hjøllum
281276-3647

Copenhagen, May 1th 2001

4 Sputtering

We are using sputtering for the manufacturing of our particles. We will therefore use the next section to describe the apparatus. There is little known about the theory behind the hollow cathode cluster source, (HCCS). The following sections are based on [17, Chapter 2][16], whose author was involved in the construction of the HCCS.

4.1 The hollow cathode cluster source

The sputtering machine consists of four vacuum chambers.

The first chamber is the condensation chamber which contains the cluster source, described in section 4.1.1. The second chamber, the sample chamber, contains a sample holder and a quartz crystal. The sample holder and the quartz crystal are placed on the sides of a plate. The plate is mounted on a metal rod so that we can turn the plate and regulate its height. The quartz crystal is a sensitive deposition sensor coupled to a monitor. A pressure sensor and a rotary pump are coupled to both the condensation chamber and the sample chamber. A nozzle connects the condensation chamber and the sample chamber. The dimensions of the nozzle are: Diameter 3.00 mm and length 50.0 mm.

Section three and four are each coupled to a turbo pump. Together these four pumps generate a pressure gradient throughout the system, with lowest pressure in chamber 4, and highest in chamber 1.

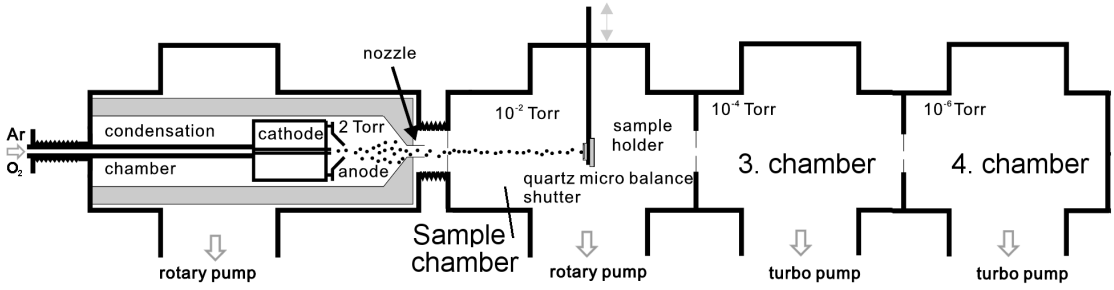

Figure 1: *The hollow cathode cluster source, schematic overview* [17]

4.1.1 The cluster source

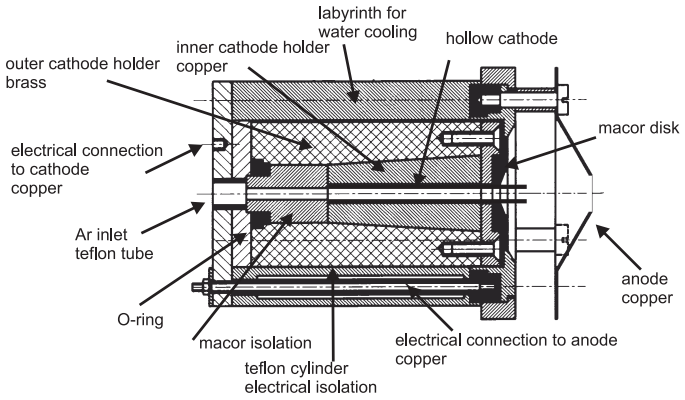

Figure 2: *The cluster source, schematic overview. Image from [17].*

In principle the hollow cathode cluster source works by condensing atoms into small particles by cooling a supersaturated metal vapour, generated by energetic ion sputtering in a hollow cathode.

The dimensions of the hollow cathode (99.998 % pure iron) are: Outer diameter 5.00 mm, inner diameter 3.00 mm and length 51.00 mm. The cathode is mounted in a conic copper and a brass block cooled by water (see 4.1.1). A "hat"- shaped copper anode with a hole in the top is mounted 10.0 mm from the cathode. This shape was chosen to avoid disturbing the gas flow in the condensation chamber. The anode and cathode are separated by ceramics in the hot regions and polymer in the cold regions. During experiments, the voltages applied to the anode, V_a are usually in the range of 0 - 10 V and the cathode, V_{cat} are usually in the range of -250 to -800 V. A gas mixture consisting mostly of argon and a certain chosen percentage of oxygen is allowed to flow through the hollow cathode and the entire system. The pressure of the gas, $P = P_{\mathrm{Ar}} + P_{\mathrm{O_2}}$, in the condensation chamber is between 0.5 Torr and 2.2 Torr, in the second chamber the pressure is $\sim 10^{-2}$ Torr and in the third chamber the pressure is $\sim 10^{-4}$ Torr. The material is produced in two ways:

1. Sputtering occurs by energy transfer of the Ar gas to the Fe-atoms in the hollow cathode
2. Evaporation of iron atoms caused by local heating.

The positive Ar ions are accelerated into the inner walls of the cathode. This bombardment releases secondary electrons, iron atoms and iron dimers and thereby building up a steady state plasma. The plasma current, I_{plas}, is typically in the range of 0.3-0.8 A.

The threshold energy of Fe-atoms in the Fe-lattice is 20 eV [17]. The impacts with higher energy knocks the iron atom out of their crystal structure. Many impacts by Ar atoms with less kinetic energy cause a local heating and causes iron atoms to evaporate. When sputtered iron atoms meet an oxygen molecule, O_2, they are quickly oxidised and iron oxide is produced. In the condensation chamber the iron oxide cools by colliding with Ar atoms. The Ar gas is cooled through collision with the outer walls of the condensation chamber.

Due to the big pressure difference between the condensation chamber and the second chamber (0.5-2 Torr and 10^{-2} Torr respectively), there is a flux of gas towards the second chamber through the nozzle connecting them. Since the nozzle is very narrow, and the difference in pressure is relatively large, a beam is formed in the second chamber. The beam consists of a mixture of Ar, O_2 and iron oxide particles.

The sample holder is aligned with the emerging beam. The only role of the oxygen is to oxidise the sputtered iron whereas the Ar has several roles. It generates a steady state plasma. It cools the sputtered material makes it cluster. It produces a flow and leads the material to the sample holder [17].

4.2 A typical run

A typical run with the HCCS consists of four steps:

1. Cleaning of the cluster source, insertion of new cathode, insertion of new quartz crystal and new sample holder.
2. The HCCS is assembled, a vacuum is created inside it, ensuring a minimal level of oxygen and water vapour.
3. When the pressure is approximately 10^{-4} Torr, heating of the HCCS is conducted. Heating consists of increasing pressure and current gradually during 90-120 mins.
4. When the HCCS has been heated sufficiently, particle production is conducted. However a (P,I)-point where particle production is stable has to be found. Thereafter the HCCS can produce particles until the cathode is exhausted, or it becomes unstable. During this part which lasts 4-8 hours, the HCCS has to be supervised regularly.

5 Mössbauer spectroscopy

5.1 Theory

In this chapter Mössbauerspectroscopy and how its data can be interpreted are described. The following sections (5.1.2 and 5.1.3) are based on notes by S. Mørup [21]

5.1.1 Hyperfine interaction

The nucleus will from it's place in the centre of the atom feel the s-electrons that orbit it, as an electric current. This results in a magnetic field.

If we sum the distribution-functions of the s-electrons, assuming shells are filled and spherically symmetric, the result will be a net zero magnetic field.

A nucleus with quantum number $I > 0$ carries a magnetic dipole moment μ. Thus it will interact with any magnetic field at the nucleus. The interaction energy between μ and a magnetic field is given by:

$$E = -\mu \cdot \mathbf{B}. \tag{5.1}$$

The magnetic interaction splits the nuclear energy into $2I + 1$ equispaced sublevels. The energy of each m-level is given by [8]:

$$E_m = -g\beta_n m B \tag{5.2}$$

where g the Landé factor, β_n is the nuclear magneton, m is the m-quantum number.

In this project only iron-oxides are of interest. ^{56}Fe has spin $I = 0$, in ground state, and hence does not interact with a magnetic field. However ^{57}Fe has a spin $I = \frac{1}{2}$, in the ground state and will therefore interact with a magnetic field.

We will be dealing with transitions between $I = \frac{3}{2}$ and $I = \frac{1}{2}$ states of ^{57}Fe. Due to hyperfine magnetic interaction, these energy levels split into 4 and 2 levels respectively. The selection rules of quantum mechanics dictate that there exist only 6 possible transitions ($\Delta I = \pm 1; \Delta m = \pm 1, 0$). Other transitions would violate conservation of angular momentum (see figure 3). We have just

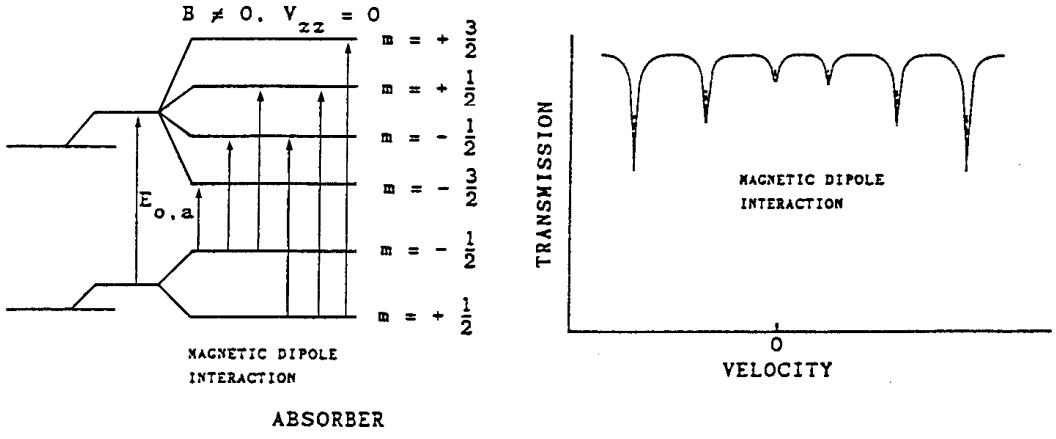

Figure 3: Left: *The 6 allowed transitions.* Right: *The corresponding Mössbauer spectrum. From [21].*

argued that the net magnetic from the s-electrons are zero. When iron forms chemical binding, the valence electron shells are deformed. Iron oxides can therefore not be considered symmetrical. The electron configuration of iron is $[\mathrm{Ar}]3\mathrm{d}^6 4\mathrm{s}^2$ [4], which means that the valence electrons are s-electrons and d-electrons. When iron has formed a chemical bond as Fe^{2+} or Fe^{3+}. The inner electron shells are deformed, and this results in a non-zero magnetic field at the nucleus, thereby

justifying (5.1). (5.1) can be generalised to

$$\mathbf{B} = \mathbf{B}_{\text{ext}} + \mathbf{B}_{\text{L}} + \mathbf{B}_{\text{D}} + \mathbf{B}_{\text{C}}, \tag{5.3}$$

where $\mathbf{B}_{\text{ext}}$ is the external magnetic field, $\mathbf{B}_{\text{L}}$ is the magnetic field arising from the orbital motion of the electrons, $\mathbf{B}_{\text{D}}$ is the contribution from the magnetic moment of the spins of the electrons, $\mathbf{B}_{\text{C}}$ is the contribution of the electron spin-density, at the nucleus arising from the s-electrons. $\mathbf{B}_C$ is often, by far, the largest contribution.

5.1.2 Electric quadrupole interaction

Nuclear states with spin $I > \frac{1}{2}$ will have a non-spherical charge distribution, and hence give rise to a quadrupole moment at the nucleus. The shift of the energy levels can be derived as follows[21, (7.1)].

The charge deformation can be described by:

$$eQ = \int \rho_n(\mathbf{r}) \cdot r^2(3cos^2\theta - 1)d\tau, \tag{5.4}$$

where Q is the electric quadrupole moment, $+e$ is the charge of a proton, and $\rho_n(\mathbf{r})$ is the nuclear charge density in the volume element $d\tau$ at the distance r from the centre of the nucleus and at an angle $d\theta$ to the nuclear spin quantization axis.

The electric quadrupole energy depends on the electric field gradient (EFG) at the nucleus. This results in a 3×3 tensor[21, (7.2-3)]:

$$EFG = \nabla E = -\nabla^2 V \quad \text{where} \quad V_{ij} = \frac{\partial^2 V}{\partial i \partial j}, \tag{5.5}$$

where $i, j = x, y, z$. If it is assumed that the order of differentiation is interchangeable, then the EFG tensor will be symmetric. Hence it can be diagonalised. Further the Laplacian (5.5) requires a traceless tensor ($\sum V_{ii} = 0$). It is therefore necessary to define the EFG by two independent properties η and V_{zz}:

$$\eta = \frac{V_{xx} - V_{yy}}{V_{zz}} \tag{5.6}$$

If the axis are arranged such that $|V_{zz}| \geq |V_{xx}| \geq |V_{yy}|$, then $0 \leq \eta \leq 1$. The tensor can be considered to be representing two contributions:

1. A *lattice contribution* arising from the charges of neighbouring ions which surround the Mössbauer atom in a non-cubic lattice.
2. A *valence electron contribution* arising from an anisotropic electron distribution in the valence shell of the Mössbauer atom.

The total contribution to the quadrupole tensor can, to a good approximation, be represented by [21]:

$$V_{zz} = (1 - \gamma_\infty)(|V_{zz}|)_{\text{slat}} + (1 - R)(|V_{zz}|)_{\text{val}}, \tag{5.7}$$

and

$$\eta = \frac{1}{V_{zz}}(1 - \gamma_\infty)(|V_{zz}|)_{\text{lat}}\eta_{\text{lat}} + (1 - R)(|V_{zz}|)_{\text{val}}\eta_{\text{val}}, \tag{5.8}$$

where γ_∞ and R are the so called Sternheimer shielding factors [21]. For Fe-atoms $1 - \gamma_\infty$ is approximately 10, whereas 1-R is of the order of 0.65-0.75. The energy levels are shifted according to the equation[21, (7.13)]:

$$E_Q = \frac{eQV_{zz}}{4I \cdot (2I - 1)}(3m^2 - I(I + 1))\sqrt{(1 + \frac{\eta^2}{3})}, \tag{5.9}$$

where m is the m-quantum number. The ground state of Fe has a spin of $I = \frac{1}{2}$ and therefore no quadrupole moment, and therefore it does not spilt. The first excited state has spin $\frac{3}{2}$ and will spilt into two components, m= $\pm\frac{3}{2}$ and m= $\pm\frac{1}{2}$ (figure 4).

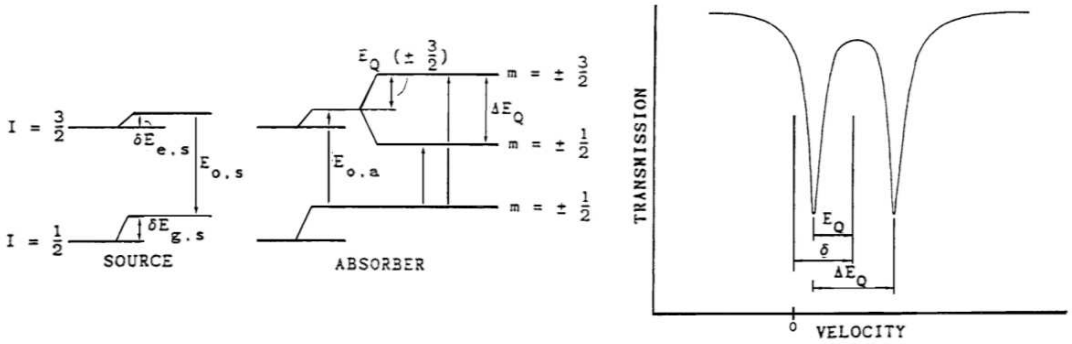

Figure 4: *The quadrupole splitting of ^{57}Fe and the effects in Mössbauer spectroscopy. Figure from [21].*

5.1.3 The isomer shift

The isomer shift arises from electric interaction between the nucleus and the s-electrons which are the only ones who have a non-zero probability of being in the vicinity of the nucleus. From [21] we get:

$$\delta E = \int_0^\infty -e|\Psi(r=0)|^2(V'-V)4\pi r^2 dr, \tag{5.10}$$

where

$$V = \frac{Ze}{4\pi\epsilon_0 r}, \quad (r>0), \tag{5.11}$$

is the electrostatic potential for a nuclear point charge Ze at a distance r, while V' (below) is the potential for a nucleus of finite size:

$$V' = \frac{Ze}{4\pi\epsilon_0 R}(\frac{3}{2} - \frac{r^2}{2R^2}), \quad (r \leq R), \tag{5.12}$$

$$V' = \frac{Ze}{4\pi\epsilon_0 r}, \quad (r \geq R). \tag{5.13}$$

Insertion into 5.10 gives:

$$\delta E = \frac{1}{10\epsilon_0} Ze^2 R^2 \Psi(0)^2. \tag{5.14}$$

The nucleus has different radii in the ground state, (R_g), and excited state, (R_e), This yields a energy difference of $\Delta E = \delta E_e - \delta E_g$. Furthermore the source and absorber usually have different chemical environments, so $|\Psi_a(0)|^2 \neq |\Psi_s(0)|^2$. Summing these components, we get the total expression for the isomer shift, δ, visualised by figure 5:

$$\delta = \frac{Ze^2}{10\epsilon_0}(R_e^2 - R_g^2)(|\Psi_a(0)|^2 - |\Psi_s(0)|^2). \tag{5.15}$$

5.1.4 Zeemann effect

If the atom is subjected to an external magnetic field we have a situation which is similar to that of the hyperfine structure. The only difference lies in the origin of the magnetic field. However the result is essentially the same. The interaction energy between μ and the magnetic field is given by (5.1).

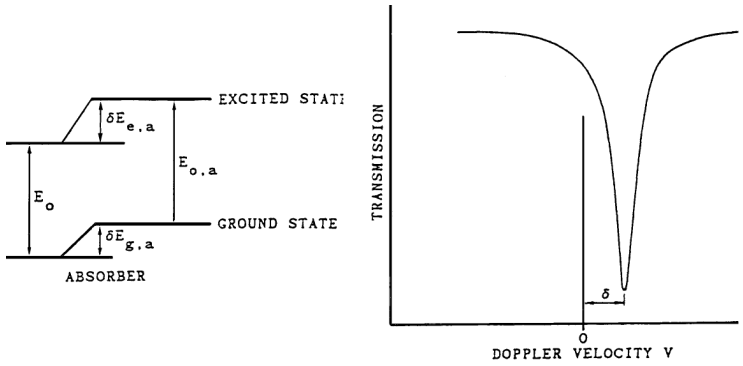

Figure 5: *The isomer shift of ^{57}Fe and its effect in Mössbauer spectroscopy. The electric monopole interaction shifts the levels without lifting the energy levels. Figure from [21].*

5.1.5 Accumulated effects

We have hitherto only dealt with four physical effects relevant to Mössbauer spectroscopy in a quantitatively manner, however the bigger picture is yet to be given. As reference we use the Mössbauer spectrum of α-Fe, i.e. Fe atoms in a pure iron crystal.

As previously mentioned the **Zeemann effect** and the **hyperfine interaction** both have the same effect on the energy levels, that is splitting the existing energylevels into 2I+1 energy sublevels. The magnitude of the splitting depends the magnetic field:

$$E_{\text{split}} = \mu \cdot (\mathbf{B}_{\text{hyperfine}} + \mathbf{B}_{\text{Zeemann}}). \tag{5.16}$$

The **isomer shift** is responsible for shifting the energy levels. It will shift all the absorption lines (and energies) by an equal amount. The **electric quadrupole interaction** is responsible for increasing the energy of the $|\frac{3}{2};\pm\frac{3}{2}>$ states and decreasing the energy of the $|\frac{3}{2};\pm\frac{1}{2}>$ states according to (5.9), if V_{zz} is positive. If V_{zz} is negative the effects are opposite. After inserting into (5.9) we get:

$$E_Q(m=\pm\frac{3}{2}) = C(-3), \quad \text{where} \quad C = \frac{eQV_{zz}\sqrt{1+\frac{\eta^2}{3}}}{4I(2I-1)}, \tag{5.17}$$

$$E_Q(m=\pm\frac{3}{2}) = C(+3). \tag{5.18}$$

This result in an increment of the energy of transitions 1 and 6, thereby moving these absorption lines to the right. The energy of the other transitions is lowered and the absorption lines move left. The six absorption lines are connected to the transitions as follows from table 1.

#	$\lvert I;m>\mapsto$	$\lvert I;m>$	#	$\lvert I;m>\mapsto$	$\lvert I;m>$
1	$\lvert\frac{1}{2};-\frac{1}{2}>\mapsto$	$\lvert\frac{3}{2};-\frac{3}{2}>$	4	$\lvert\frac{1}{2};+\frac{1}{2}>\mapsto$	$\lvert\frac{3}{2};-\frac{1}{2}>$
2	$\lvert\frac{1}{2};-\frac{1}{2}>\mapsto$	$\lvert\frac{3}{2};-\frac{1}{2}>$	5	$\lvert\frac{1}{2};+\frac{1}{2}>\mapsto$	$\lvert\frac{3}{2};+\frac{1}{2}>$
3	$\lvert\frac{1}{2};-\frac{1}{2}>\mapsto$	$\lvert\frac{3}{2};+\frac{1}{2}>$	6	$\lvert\frac{1}{2};+\frac{1}{2}>\mapsto$	$\lvert\frac{3}{2};+\frac{3}{2}>$

Table 1: *The six allowed transitions and the corresponding absorption lines.*

5.1.6 Experimental application

We have a photon source that emits γ-photons that have an energy of approximately 14.4 keV. A small portion of the photons will be absorbed by the ^{57}Fe-nuclei, and then remitted in an arbitrary direction. If a detector is placed behind the sample, a small decrease in the number of photons, at the energies corresponding to the 6 allowed transitions, is observed.

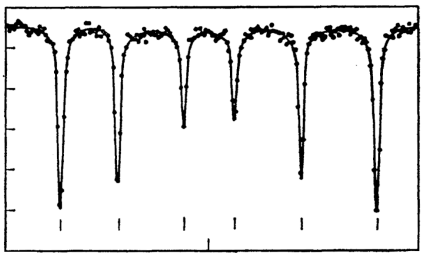

Figure 6: *A typical Mössbauer spectrum (here hematite α-Fe_2O_3) with a well developed sextet. Figure from [21].*

As source we use ^{57}Co which has a lifetime of 270 days. It decays to ^{57}Fe$^{**}(I = \frac{5}{2})$, which again in 90% of the cases decays, to a intermediate state of ^{57}Fe$^{*}(I = \frac{3}{2})$ and 10% to ^{57}Fe$(I = \frac{1}{2})$. When ^{57}Fe* decays to ^{57}Fe it emits a γ-photon of 14.4keV (see figure. 7).

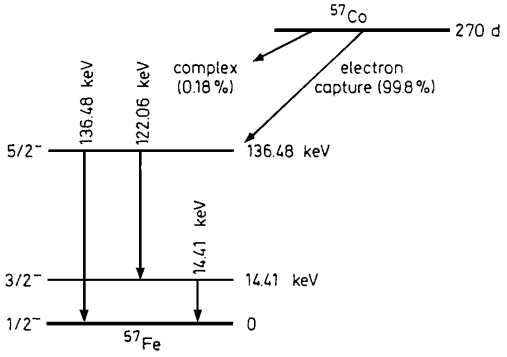

Figure 7: *The Decay of ^{57}Co to ^{57}Fe. Figure from [21].*

5.2 Apparatus

In this section we will present the apparatus, that is used for our Mössbauermeasurements. The apparatus consists of 3 parts:

1. The drive unit with a velocity transducer containing the radioactive source.
2. The MCA[2].
3. Detector and SCA[3].

5.2.1 Drive unit

The energy of the photon emitted when the ^{57}Fe* atom decays to ^{57}Fe, is approximately 14.4 keV. In Mössbauer spectroscopy we are concerned with the small variation around this energy. The source is mounted at the end of a rod that is attached to two electro magnets. The energy variation is obtained by oscillating the radioactive source with a constant acceleration in each direction, taking advantage of the Doppler effect. One of the electro magnets is feed appropriate voltage; this results in an oscillating motion of the rod. The current induced in the others coil is

[2] Multichannel analyser
[3] Single channel analyser

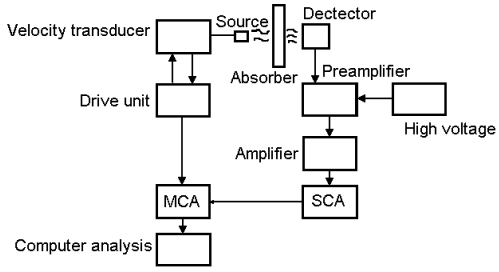

Figure 8: *Schematic overview of the Mössbauer apparatus setup. Slightly modified from [21, fig. 13.1]*

proportional to the velocity of the rod. This current is used in an electric feedback system, and ensures that the velocity is precisely controlled [21]. A typical maximum velocity of the source is $\sim$10 mm/s.

5.2.2 Detector

The detector is essentially a Geiger-Müller detector. When it registers the incoming photons it sends a pulse to the pre-amplifier, which again sends it to the amplifier. The amplifier is connected to a SCA which is connected to a MCA, which in turn is coupled to a computer.

5.2.3 MCA

The role of the MCA is to sort the incoming photons into channels according to their energy. Each channel contains the number of photons received within a specified energy interval. We use a 1024 channel MCA[4].

Although the detector is a Geiger-Müller detector, it is possible to give a rough estimate of the energy of the incoming photon. This resolution is however far from accurate enough to resolve the energy differences that are measured using Mössbauer spectroscopy. The detector is able to resolve approximately 0.1keV. A typical Mössbauer Doppler energy perturbation is 10 mm/s. The velocity is non-relativistic so the energy perturbation can be derived from[21, (3.7)]:

$$\Delta E = E_0 \frac{v}{c}, \quad E_0 = 14.4\text{keV}, \tag{5.19}$$

where v is the velocity of the source and c is the velocity of light in vacuum. Inserting into (5.19), one gets $\Delta E = 4.8 \cdot 10^{-10}$ keV, which is far from the resolution of the detector.

To sort the pulses the MCA has to receive data from both the detector and the drive unit. By reading the velocity of the source when a pulse is received, the MCA calculates which channels count should be increased. The MCA is thereby able to sort the incoming pulses.

The accumulated data can be read from the MCA, into a computer for processing, if desired. Typical timespan for a Mössbauerexperiment is 4 hours to 2 weeks depending on how thick the sample is, how radioactive the source is, the geometry of the system and finally the desired certainty. On the MCA, an energy window is set, so that only the pulses with energy around 14.4keV are registered.

6 Experiment

6.1 Manufacturing the particles

The particle production was the most time consuming part of this project. So we feel that it is justified to spend some time describing the manufacturing process, samples, theory and apparatus.

[4] 512 or 1024 channels are the most common [19].

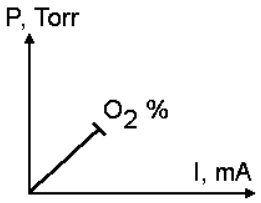

Figure 9: *The P,I,[O_2] in which we are to determine suitable parameters in order to get the hollow cathode cluster source to produce nano-sized iron oxides.*

Controlled oxidation using sputtering in the HCCS, is opposed to Mössbauer spectroscopy, an unknown field. A great deal of our work effort therefore lies in this part of the experimental work. The task presented to us had several aspects: finding a gas mixture containing a amount of O_2, the HCCS is able to produce particles, finding (for each gas mixture) a current and a pressure at which the HCCS is able to run. This was essentially a problem with 3 degrees of freedom illustrated by figure 9.

6.1.1 Initial strategy

To set up a useful strategy for the nano-particle production a few known facts should be taken into consideration:

1. Experiments performed at HCØ have shown that it is possible (although hard) to produce iron oxides in the sputtering machine using gas mixture of 98%Ar and 2% O_2 [16].
2. It is relatively easy to produce Fe-particles with a thin oxide layer, using sputtering, with pure Ar gas. The O_2 for the oxidation comes from leakage in the system [16].
3. Since temperature is high (∼1300K) [16], and pressure is low (∼1Torr=133Pa), we can consider the gas inside the condensation chamber as ideal. Furthermore most of the gas is Ar which is ideal i.e. consist of mono-atomic molecules.
4. Iron oxidises very fast.
5. The temperature of the plasma in the sputter source is very high, and chemical reactions are thus fast.
6. The purpose of our experiments was to produce small particles, with a diameter less than 10 nm.
7. Iron-oxides are very willing to cluster, and therefore form large particles.

Since experiments at HCØ, showed that it was possible to produce particles with Ar-mixtures containing 0 % and 2 %, we decided to start with a mixture of 0.2 %. The reason we did not use 1.0 % was to keep reaction time low, as we assume that reaction speed would increase with higher oxygen level.

Should this prove unsuccessful, we planned increasing the oxygen level to 2.0 % O_2.

6.2 Sample requirements

Due to the nature of Mössbauer spectroscopy the quality of the measurement lies in how much of the radiation is absorbed and remitted. Therefore there are certain requirements for a sample. An area of approximately half the area of the sample holder is to be covered. An area is considered covered when it is impossible to see sharp light through it, using magnifying lenses.

6.3 Course of action

Following the strategy outlined in (6.1.1), we were - with much effort - able to produce a single usable sample (JK003)[5] using 0.2% O_2.

The 2.0% O_2 mixture proved worthless, the problems were:

- Unstable plasma, which is seen as fast violent fluctuations in both voltage and current.
- No particle production, or unstable particle production, ranging from very low to very high levels.

It was only possible to obtain particle production (0.2% O_2) using very high currents($\sim$ 0.600-0.900 A and thus high temperature), and pressure($\sim$ 1.8-2.3 Torr) in the condensation chamber. Under these circumstances a cathode is short lived and lasts only for 6-8 hours. Thus the cathode has to be changed a least once, since a typical run takes 8-12 hours.

Considering the problems manufacturing the particles using 0.2% O_2 and failure at higher percentage of O_2, and that Kuhn [16][17] had produced Fe-particles using pure Ar, a lower percentage of oxygen was tried. We decided on 0.02% O_2 in Ar, trying to get closer to a gas mixture, that had the positive properties of Ar, while still containing a big enough percentage O_2 to get fully oxidised particles.

Stable particle production was easy using 0.02% O_2. Furthermore the current and pressure necessary for particle production were low, $\sim$0.350-0.400 A, and $\sim$1.3-1.7 Torr, thereby increasing the lifetime of a cathode by a factor 4-5[6]. The samples produced with this gas mixture are: JK006 & JK011. We performed a control-run with pure Ar, and the resulting sample was JK010. Data for the samples, and the circumstances under which the particles were produced are listed in table 2. The area in which stable particle production was achieved are illustrated in figure 10.

Sample name	O_2 molar %	Ar molar %	U_{cat} V	I_{cat} mA	Pressure Torr	Particle deposition Å/s	Time min
JK003a	0.2	99.8	371-379	640-855	2.0-2.2	0.4-0.9	240
JK003b	0.2	99.8	370-375	650-843	2.0	0.4-1.6	210
JK010	0.0	100.0	295-332	531	1.0	0.1-3.4	270
JK011a	0.02	99.98	342-344	400	1.5	5-12	70
JK011b	0.02	99.98	342-344	350-400	1.4	3.2-4.9	360

Table 2: *The circumstances under which our samples were manufactured. The letters a,b indicate that the sample was produced in 2 runs, because it was necessary to stop the run for a while (<30 min), since the deposition sensor crystal was overloaded, and needed to be replaced. The pressures indicated are measured in the condensation chamber.*

7 Theory of small iron oxide particles

Before describing the different types of magnetic phases we will begin with a short introduction to anisotropy energy followed by paramagnetism, ferromagnetism, antiferromagnetism, ferrimagnetism and finally superparamagnetism.

7.1 Anisotropy

It is easier to magnetise a crystal in some directions than others. These easy magnetisation directions depend on the anisotropy of the crystal. The direction in which the magnetisation requires most energy is called the hard direction of magnetisation. The anisotropy energy is the

[5] We will be referring to the samples by the name given in the laboratory during manufacturing. Only potentially successful samples were numbered.

[6] We were able to do 3 runs, each lasting 8-12 hours, on a single cathode using this gas mixture

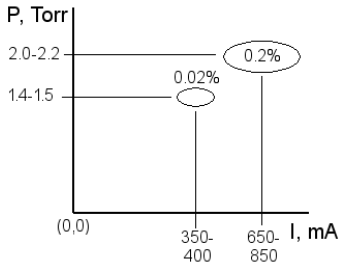

Figure 10: *A schematic view of the elliptic areas in the P-I-plane in which stable particle production was possible. The search was performed in the entire indicated part of the plane.*

energy related to turn the magnetisation away from the easy magnetisation direction. Anisotropy has its origin in different physical quantities. We will discus exchange energy, crystal anisotropy and shape anisotropy because these are the dominating anisotropies [5].

The **exchange energy** is due to spin-spin coupling. The exchange energy is a very strong short-ranged force and its hamiltonian is represented by [14]:

$$H = -2J \sum \mathbf{S}_i \cdot \mathbf{S}_j, \tag{7.1}$$

where J is the energy integral and $\mathbf{S}_i$,$\mathbf{S}_j$ are the spin vectors. If J is negative then parallel spins are energetically favourable. If J is positive then antiparallel spins are energetically favourable [6]. Therefore exchange energy tends to align the spins parallel or antiparallel. Exchange energy has no direct contribution to anisotropy. However the strong spin-spin coupling is linked to a certain orientation through the crystal anisotropy.

Crystal anisotropy is due to spin-orbit coupling. For cubic crystal structures the orbital angular momentum is almost quenched. This means that the orbits are strongly fixed to the lattice and there is no net orbital magnetic moment ($L = 0$). Hence the Landé factor given by [13]:

$$\mathrm{g} = 1 + \frac{\mathrm{J(J+1)} + \mathrm{S(S+1)} - \mathrm{L(L+1)}}{2\mathrm{J(J+1)}}, \tag{7.2}$$

which is approximately 2, where $J = S + L$. The effect of the spin-orbit coupling is to couple the spin to the lattice.

Shape anisotropy is due to dipole-dipole interaction. In an ellipsoidal (or prolate spheroid) nano particle the dipole-dipole interaction will force the dipoles to align along the major axis of the particle. The magnetic field from a dipole is, in coordinate free form, given by [7]

$$\mathbf{B}_{\mathrm{dip}}(\mathbf{r}) = \frac{\mu_0}{4\pi}\frac{1}{r^3}[3(\mu \cdot \hat{\mathbf{r}})\hat{\mathbf{r}} - \mu], \tag{7.3}$$

where μ is the dipole moment. If the dipole moments are parallel to a minor axis, there will be an overall demagnetisation of the particle. The effect of this demagnetisation is to align the dipole moments antiparallel. This requires the presence of a block wall. For single domain particles this is not possible (see section 7.2). Hence the magnetic dipoles are aligned along the major axis.

If the anisotropy of a particle is uniaxial the magnetic energy can be approximated by:

$$E(\theta) = KV \sin^2\theta, \tag{7.4}$$

where K is the magnetic anisotropy constant, V is the volume of the particles and θ is the angle between the magnetisation and the easy magnetisation direction [8][21]. From (7.4) we get that two arbitrary energy minima are separated by a energy barrier of height KV. From [8] we get that the probability f of the angle θ being between θ and $\theta + d\theta$ is given by the Boltzmann distribution:

$$f(\theta)d\theta = \frac{\exp(\frac{-E(\theta)}{k_{\mathrm{B}}T})\sin(\theta)d\theta}{\int_0^{\frac{\pi}{2}} \exp(\frac{-E(\theta)}{k_{\mathrm{B}}T})\sin(\theta)d\theta} \tag{7.5}$$

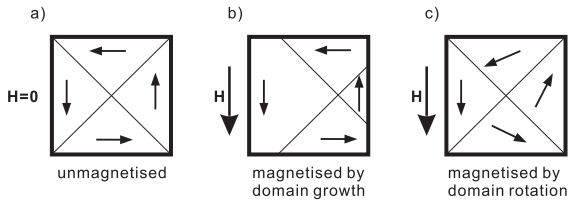

Figure 11: *Different kinds of domain magnetisation. Figure from [17].*

The relation between $k_{\mathrm{B}}T$, KV and the magnetic moment of the particle is:

$k_BT \ll KV$**:** $f(\theta)$ is large around $\theta = 0$, and therefore the magnetic moment is fixed around the easy direction of magnetisation. In the Mössbauer spectrum this is seen as a narrow absorption line.

$k_BT \simeq KV$**:** For these values the magnetic moment fluctuates around the easy directions of magnetisation, and has a small probability of crossing the energy barrier. In the Mössbauer spectrum this is seen as a broad absorption line. The absorption lines can become hard to distinguish, due to overlap.

$k_BT \geq KV$**:** For these values the thermal energy is high enough for the magnetic moment to have a possibility of crossing the energy barrier. This phenomenon is known as superparamagnetic relaxation, which is characterised by the relaxation time τ. τ is the mean time between two passages of the energy barrier. The absorption lines will be indistinguable, due to changes in the direction of the magnetic moment.

7.2 Domain theory

Domains are regions in magnetic matter, where all the magnetic moments are aligned. These will act as powerful dipoles. At a certain particle size the dipole-dipole interaction will dominate the exchange interaction.

Whether a particle is a multi domain or single domain is a balance between dipole and exchange energy. For a particle in which all the magnetic moments are aligned, the total dipole will generate a large external magnetic field in a large volume. By division into domains, the energy in the external magnetic field is reduced. This is done on expense of an increase in the exchange energy inside the block wall. The splitting into domains is a result of the minimisation of the total energy, i.e. the dipole magnetic energy and exchange energy.

The block wall is the transition layer between two domains with non-parallel magnetic moments, where the local magnetic orientation is gradually changed. The width of a block wall is independent of particle size [14], it is determined by the exchange interaction and the anisotropy energy.

Magnetisation of a multi domain particle is done either by block wall displacement, also called domain growth, or domain rotation. When particles are sufficiently small (diameter in the range from 1 nm to 100 nm [17]), it is not energetically favourable to maintain a multi domain. Reversal of magnetic moment by an applied field can only be achieved by coherent or incoherent domain rotation, fanning, curling and buckling.

For small particles the fraction $\frac{S}{V}$, where S is surface and V is volume, is very large. Therefore a large fraction of the atoms will be near the surface, and thereby lacking some neighbouring atoms, giving rise to a decreased exchange energy. This causes a greater susceptibility to thermal agitation of the magnetic moments.

7.3 Magnetic phases

7.3.1 Ferromagnetism

Ferromagnetics are characterised by their spontaneously alignment of atomic magnetic moments, despite an external field. The origin of ferromagnetics is exchange forces, with $J < 0$. Due to thermal agitation (T$>$ 0 K) the magnetic moment will not be perfectly aligned. As the temperature increases, the magnetic moments tends to fluctuate gradually more violently. This causes the magnetisation to decrease gradually. When the thermal agitation exceeds the exchange energy, there is no total magnetic order, and the material becomes paramagnetic. This point is called the Curie temperature, T_C. Because of the hypefinestrucure, ferromagnetics below the Curie temperature are in Mössbauer spectrum seen as sextets. Above T_C ferromagnetics become paramagnetic and are seen as a singlet/doublet depending on whether a quadrupole moment is present or not.

7.3.2 Antiferromagnetism and ferrimagnetism

In antiferromagnetic materials the magnetic moments are antiparallel, thereby cancelling each other, the total magnetic moment is zero. As in ferromagnetism, the atomic magnetic moment will fluctuate due to thermal agitation. When the temperature reaches the Néel temperature, T_N, the magnetic order has been destroyed, and the material behaves paramagnetic. In Mössbauer spectra antiferromagnetics below T_N are seen as sextets, due to hyperfine splitting.

In ferrimagnetics the spins are aligned antiparallel, but the atomic magnetic moment is stronger in one direction, than the opposite. They behave magnetically like ferromagnetics, and are in Mössbauer spectra seen as sextets. Above the Curie temperature they become paramagnetic.

The origin of both antiferromagnetism and ferrimagnetism is exchange forces, but with $J > 0$, thereby favouring antiparallel spins. Above T_N/T_C both atniferromagnetics and ferrimagnetics are seen as singlets/doublets.

7.3.3 Paramagnetism

When the temperature of a magnetically ordered material is increased, the magnetic moments in the particle will fluctuate more violently. This causes the external magnetic moment to decrease gradually, eventually becoming zero.

In an external field the atoms will tend to point in the direction of the field. But thermal agitation of the atom opposes this tendency and tends to keep the atomic moments pointed at random. This results in a partial alignment along the field direction and gives rise to a small positive susceptibility. In the absence of an external field the atomic magnetic moment, μ, will point at random and cancel each other. Paramagnetic iron oxides are in Mössbauer spectroscopy seen as a singlet or a doublet.

7.3.4 Superparamagnetism

When the observed particles become as small or smaller than the dynamic single domain size, the particles become superparamagnetic. This means that the thermal energy is as large, or larger than the magnetic energy. The magnetic moments of the particles are therefore no longer locked to the crystal. The magnetic moment of the particle will therefore fluctuate freely around the easy magnetisation directions. Superparamagnetism occurs when the particle sizes are less than approximately 10-100 nm.

In order to destroy the superparamagnetism of the particle, and make it magnetic, the thermal energy must be lower than the magnetic energy. This is done by either lowering the thermal energy of the particle, or by increasing the magnetic energy of the particle, by applying an external magnetic field [17].

In Mössbauer spectroscopy superparamagnetism is seen as a singlet/doublet in materials in which one would expect to see a sextet. The quantitative explanation for this effect lies in superparamagnetic relaxation.

7.3.5 Superparamagnetic relaxation

From Mørup 1982 [24] we get the following expression for the Superparamagnetic relaxation time τ:

$$\tau = \frac{M\sqrt{\pi}}{Kg\mu_B}\sqrt{\frac{KV}{k_BT}}\cdot e^{\frac{KV}{k_BT}}, \tag{7.6}$$

which can be approximated to the Arrhenius relation [17]

$$\tau = \tau_0 e^{\frac{KV}{k_BT}} \quad \text{when} \quad KV \geq k_BT, \tag{7.7}$$

where M is the magnetisation, V is the volume of the particle, K is the anisotropy constant, k_B is Boltzmann's constant, T is the temperature, $\tau_0 = \frac{M\sqrt{\pi}}{Kg\mu_\mathrm{B}}\sqrt{\frac{KV}{k_\mathrm{B}T}}$ is the characteristic time, typically $\tau_0 \approx 10^{-11}$ s.

According to (7.5) the magnetisation vector may fluctuate (collective fluctuations) in directions close to the easy direction of magnetisation, unless the parameter KV is large compared to the thermal energy. This kind of fluctuation is fast compared to the time scale of Mössbauer spectroscopy. Therefore, the observed magnetic field is the average hyperfine field:

$$B_{obs} = B_0 < \cos\theta > \quad \text{where} \quad < \cos\theta > = \int_0^{\frac{\pi}{2}} \mathrm{f}(\theta)\cos\theta \mathrm{d}\theta, \tag{7.8}$$

where B_0 is the magnetic hyperfine field in absence of fluctuations. Equation (7.8) can be approximated by:

$$B_{obs} = B_0(1 - \frac{k_BT}{KV}) \quad \text{when} \quad KV \gg k_BT. \tag{7.9}$$

At low temperatures the field observed in microcrystals decreases with temperature faster than bulk material. The maximum reduction of B_{obs} is in the order of 5-15 %. When the reduction reaches this level, the hyperfine field collapses to zero, due to fast supermagnetic relaxation. The temperature at which B_{obs} collapses, is called the blocking temperature T_B. The blocking temperature is defined as the temperature below which the relaxation time is slow compared to the observation time. This means that detection of superparamagnetism depends on the observation time in the experiment[7]

When the hyperfine field is zero, there is no splitting of the energy levels, and therefore only a singlet/doublet is observed.

7.4 Iron oxides

Since our goal was to manufacture iron oxides, we will go through the properties of the most common iron oxides.

A common iron oxide is **hematite** (α-Fe_2O_3). At temperatures ranging from 0 K to 260 K it is a weak ferromagnet, and above 260 K it is an antiferromagnet [17]. It is unstable in air at temperatures above 1700 K [12]. It has a Curie temperature of 948 K.

Another common iron oxide in nature is **maghemite** (γ-Fe_2O_3). Although it has the same chemical formulae, it differs from hematite in many aspects. It has a different crystal structure. It is a ferrimagnet. The Curie-temperature of maghemite is 948 K. It is unstable in air at temperatures above 1700 K [12].

Magnetite, ($[Fe^{3+}[Fe^{3+}Fe^{2+}]O_4]$, Fe_3O_4) is fairly common, but the oxidisation level is lower than hematite/maghemite, and can therefore be oxidised further. It is a ferrimagnet, and its Curie temperature is 851 K. Magnetite has some rather strange properties in Mössbauerspectroscopy. The outer Fe^{3+} in the formula $[Fe^{3+}[Fe^{3+}Fe^{2+}]O_4]$ is seen as a sextet (magnetite A). The two inner Fe-ions exchange an electron in a time similar to the characteristic observation time of

[7] The observation time in Mössbauer spectroscopy is the mean lifetime of the excited ^{57}Fe-nucleus with $I = \frac{3}{2}$. It is found in Appendix D as $\tau_{\frac{3}{2}}$.

Mössbauer spectroscopy. Therefore these atoms are seen as two $Fe^{2.5+}$ which also are seen as a sextet (magnetite B). This is illustrated in figure 12. Mössbauer data for hematite, maghemite and magnetite are listed in table 3. At the lowest oxidisation level we have **wüstite**, FeO, which

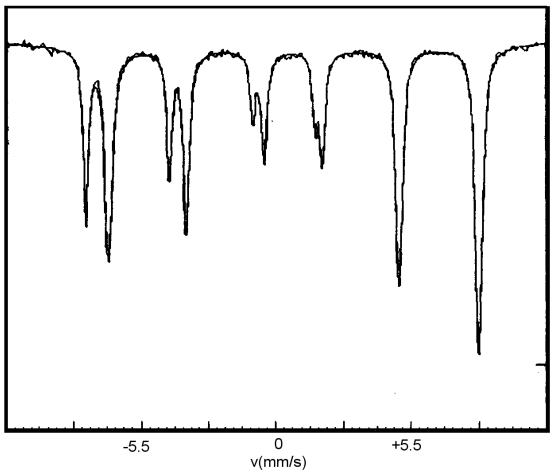

Figure 12: *A typical Mössbauer spectrum of magnetite, $[Fe^{3+}[Fe^{3+}Fe^{2+}]O_4]$, at 295 K. The two sextets are clearly visible. Figure from [26].*

Name	δ mm/s	E_Q mm/s
Hematite, α-Fe_2O_3	0.37	-0.1
Maghemite, γ-Fe_2O_3	0.32	0.01
Magnetite A Fe_3O_4	0.26	-0.01
Magnetite B Fe_3O_4	0.67	0.0

Table 3: *Tabular values of the isomer shift and quadrupole splitting for some iron oxides. Values from Macfit [2].*

is metastable below 843 K [10]. It is an antiferromagnet. It occurs with two different formulas, stoichiometric wüstite (FeO) and non-stoichiometric wüstite ($Fe_{1-x}O$; $0 < x \leq 0.15$). Its Néel temperature is given in [3] as between 186 K and 190 K. We have not been able to find literature on wüstite below the Néel temperature, but the theory [19] predicts that it splits into a sextet in the Mössbauer spectrum, since it is an antiferromagnet. Mössbauer data for wüstite from literature is listed in table 4.

Reference	Component	δ mm/s	E_Q mm/s
Park et al. [10]	$Fe_{1-x}O$	0.98	0.66
Murin et al. [22]	FeO	1.06	0.29
	$Fe_{1-x}O$	0.86	0.74
Pattek-Janczyk et al. [1]	FeO	1.03-1.07	0.28-0.32 (0.57)
	$Fe_{1-x}O$	0.90-0.96	0.71-0.76

Table 4: *Selected Mössbauer data for wüstite, found in the literature.*

8 Experimental results

The spectra have been fitted by means of the computer program MacFit [2]. Due to incapability of Mössbauer measurement software and MacFit it was necessary to construct a converter computer program [9]. The converter does not perform any data analysis, it simply converts from one file format to another.

During the fitting process we have maintained the 3:2:1 relationship between the sextets, which the theory [21] prescribes. Each absorption line is fitted using the Lorentzian distribution, given by [8]:

$$L_{Lor}(v) = \frac{I_0}{1 + \left(\frac{2(v-v_0)}{W}\right)^2}, \tag{8.1}$$

where I_0 is the maximum intensity, W is the full width half maximum, v_0 is the centre of distribution. The area of the absorption line is

$$A_{Lor} = \frac{I_0 W \pi}{2}. \tag{8.2}$$

8.1 Mössbauerspectroscopy complications

Prior to the analysis it was discovered, that there had been a major flaw in our equipment during the measurements of the spectra of JK010 and JK011 at 295 K. The error was that the source had not been sufficiently attached to the rod connecting it to the speakers, causing the source not to follow the oscillation of the rod entirely.

Furthermore there was a resonant ringing in the oscillator. This is caused by the architecture of the system, which is a mechanical swinger with a electronic feedback system. By accident a resonant frequency was struck and developed resonance.

These effects cause a significant widening of the absorption lines. An estimate of this widening, bases on the calibration spectra, is of the order 0.3-0.5 mm/s. This makes the analysis of the obtained spectra difficult and also inaccurate, since the spectra appear noisy.

8.2 The iron sample, JK010

This sample was manufactured using pure argon. It serves as a control sample.

8.2.1 Analysis of the 295 K-spectrum

Component name	Type	δ mm/s	E_Q mm/s	Width mm/s	Area %	Intensity %	Mark
Iron α-Fe	Sextet	0.000	0.000	-	53.734	-	A
Iron α-Fe *	Singlet	0.000	-	0.544	21.910	0.881	B
Wüstite $Fe_{1-x}O$	Doublet	0.817	0.730	0.942	24.599	0.286	C

Table 5: *The found components of Mössbauer spectrum of JK010 at 295K. The * indicates a superparamagnetic component. The misfit was 14.2 %.*

The spectrum (figure 13) shows presence of several (probably three) components.

1. "Macroscopic" iron particles. By macroscopic particles we understand not superparamagnetic, d> 12 nm [16]. The spectral lines are indicated and marked as A. This iron phase is present at about 54 % of the total area.

2. Superparamagnetic iron particles. The spectral line is indicated and marked as B. This iron phase is present as about 22 % of the total area.

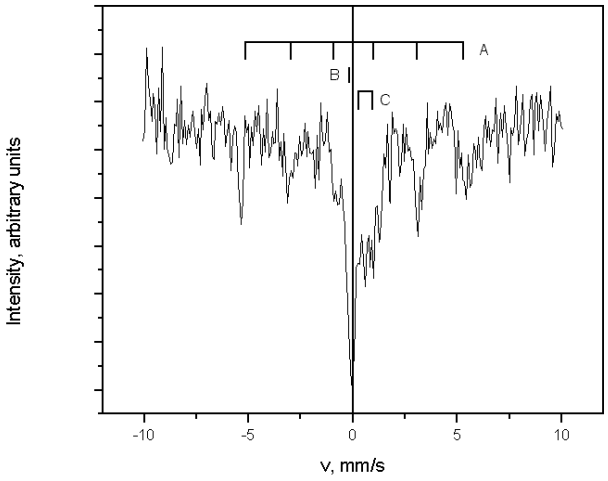

Figure 13: *Mössbauer spectrum of JK010, manufactured using pure argon, at 295 K and 0.0 T.*

3. In the centre of the shown spectrum there appears to be a third phase. This phase has not been definitely identified. It can be fitted with about 25 % non-stoichiometric wüstite. See also section 8.3.1. Another possibility is that it is magnetite (see section 8.7).

The result of the fitting is listed in table 5.

8.3 Iron oxide sample, JK011

8.3.1 Analysis of the 295 K-spectrum

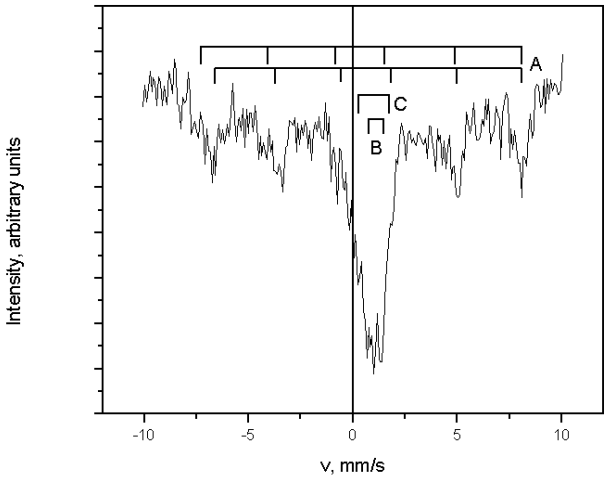

Figure 14: *Mössbauer spectrum of JK011, manufactured using 0.02 % O_2, at 295 K and 0.0 T.*

The figure (14) shows Mössbauer spectra of the particles manufactured by sputtering using a gas mixture composed of 99.998 % Ar and 0.02 % O_2. The spectrum shows presence of three

Component name	Type	δ mm/s	E_Q mm/s	Width mm/s	Area %	Intensity %	Mark
Magnetite A Fe_3O_4	Sextet	0.260	-0.010	-	5.922	-	A
Magnetite B Fe_3O_4	Sextet	0.670	0.000	-	40.582	-	A
wüstite FeO	Doublet	1.039	0.354	0.784	12.922	0.231	B
wüstite $Fe_{1-x}O$	Doublet	0.790	0.828	1.599	40.638	0.356	C

Table 6: *The found components of Mössbauer spectrum of JK011 at 295K. The misfit was 5.6 %.*

components:

1. Magnetite is marked A. Magnetite is present as about 46 % of the total area.
2. Stoichiometric wüstite is marked B and is present at about 13 % of the total area.
3. Non-stoichiometric wüstite ($Fe_{1-x}O$) is marked C and is present as about 41 % of the total area.

The result of the fit is listed in table 6.

8.3.2 Analysis of spectra of JK011 at 14 K and 200 K

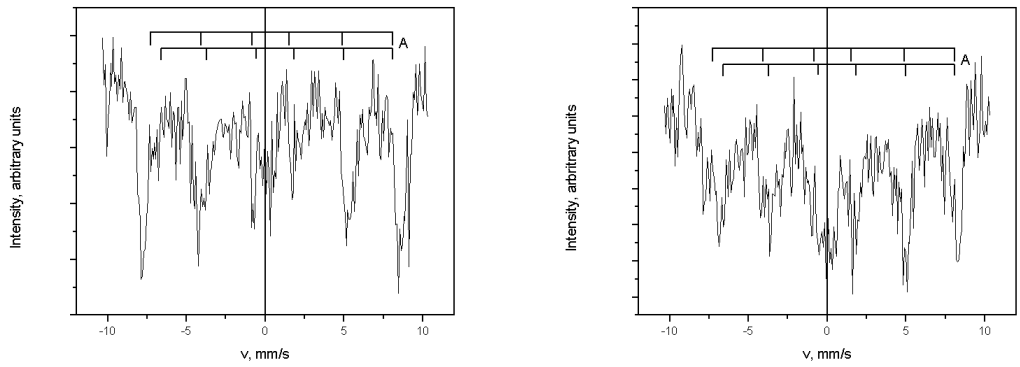

Figure 15: Left: *The Mössbauer spectrum of a sample produced using 0.02 % O_2 at 14 K.* Right: *The Mössbauer spectrum of a sample produced using 0.02 % O_2 at 200 K. The placement of the absorption lines of mangetite (Fe_3O_4) at 295 K is marked for reference as A.*

The analysis of the 295 K-spectrum indicated that wüstite is a major part of the material in the sample. The Néel temperature of wüstite is 186-190 K [3]. Below this temperature, the wüstite-doublets in the Mössbauer spectrum should split into sextets.

The 14 K spectrum (figure 15 left) shows indication of several sextets. It is known from the 295 K spectrum that magnetite(Fe_3O_4) is a major component. From [21] we know that magnetite has at least 5 sextets at 14 K. It is therefore difficult to fit, and we have not been able to find any fitting parameters. Wüstite has two different components, non-stoichiometric and stoichiometric, and thereby has at least 2 sextets at 14 K.

The temperature 200 K was chosen, because it lies just above the Néel temperature of wüstite. According to theory the spectrum should contain the doublet seen at 295 K. The 200 K spectrum (figure 15 right) shows indication of several sextets. Furthermore it shows a increase in the absorption around 0 mm/s, relative to the 14 K spectrum. However the isomer shift is lower than that of the 295 K-spectrum. We do not have an explanation for this behaviour. At one point we considered if wüstite might be destroyed in the cooling process. A control measurement, with the

JK003, which had been subjected to the same cooling process, and thereafter heated to 295 K, showed that wüstite abundance is unaffected by cooling. This spectrum is shown in Appendix C.

Thus wüstite splits into sextets, and is present in the shown spectra. We have not been able to fit the shown spectra due to its complexity.

The indicated sextets in figure 15, is the placement of 295 K-magnetite.

8.4 Iron oxide sample, JK003

8.4.1 Analysis of the 295 K-spectrum

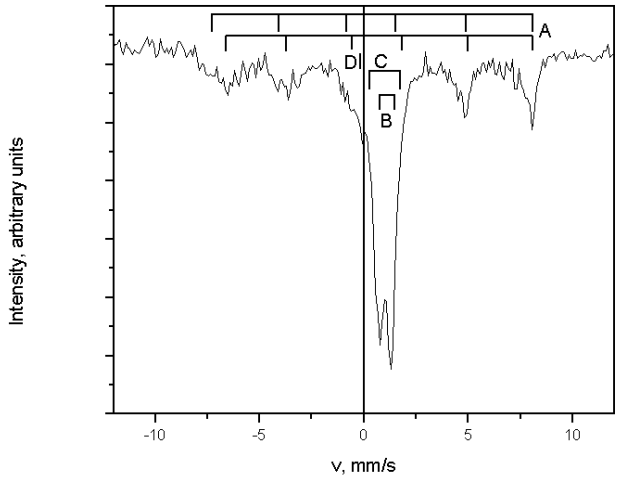

Figure 16: *Mössbauer spectrum of JK003, manufactured using 0.2 % O_2, at 295 K, 0.0 T.*

Component name	Type	δ mm/s	E_Q mm/s	Width mm/s	Area %	Intensity %	Mark
Magnetite A	Sextet	-	-	-	6.272	-	A
Magnetite B	Sextet	-	-	-	44.013	-	A
wüstite FeO	Doublet	1.036	0.432	0.453	19.201	0.345	B
wüstite $Fe_{1-x}O$	Doublet	0.960	0.730	0.527	26.411	0.407	C
α-Fe *	Doublet	-0.088	0.011	0.574	4.103	0.058	D

Table 7: *The found components of Mössbauer spectrum of JK003 at 295K. The * indicates a superparamagnetic component. The misfit is 1.7 %.*

The Mössbauer spectrum (figure 16) shows presence of four components:

1. Magnetite, Fe_3O_4, is marked A. It is present at about 50 % of the total area.
2. Stoichiometric wüstite, FeO, is marked B, and is present at about 19 % of the total area.
3. Non-stoichiometric wüstite, $Fe_{1-x}O$, is marked C, and it is present at about 26 % of the total area.
4. Superparamagnetic iron, α-Fe, is marked D an is present at about 4 % of the total area.

The result of the fitting process is listed in table 7.

8.5 Particle growth

It is not known how the iron-oxide particles are actually created inside the sputter source, but we will try to outline the most probable formation process. There are two processes that should be considered:

1. The iron atoms gather to form small particles, and are thereafter oxidised, all inside the condensation chamber.
2. The sputtered free iron atoms are oxidised immediately, to form an iron oxide. This forms small particles of iron oxides.

Initially both options are possible, or a combination of both.

Our first analysis indicates that something as unusual as wüstite exists in the sample. Therefore we have to do a careful analysis before jumping to conclusions. A comparison of values found with values in table 4 indicates that our analysis could be correct.

According to Park et al. [10], all mentioned iron oxide particles can exist at 1300K.

By the Caberra-Mott model of oxidation the rate of oxide layer growth on iron is given by [23]:

$$\frac{dx}{dt} = A\exp\Big(\frac{-x_0}{x}\Big) \Rightarrow t = A^{-1}\Big(\frac{x^2}{x_0}\Big)\exp\Big(\frac{-x_0}{x}\Big), \tag{8.3}$$

where at 295 K, A$\simeq 5.4 \cdot 10^{-30}$ m/s and $x_0 \simeq 8 \cdot 10^{-8}$ m. Here we have used the parameters for iron, since those for wüstite are unknown. At 295 K this results in that it takes ∼1 fs to produce an oxide-layer of 1 nm, ∼40 s to produce 2 nm. By this model the surface oxidisation is very fast, and decreases very rapidly inwards. Seen in the light of this, it is most likely that the process of manufacturing particles follows the path outlined in 2.

It must be taken into account, though, that the particles are formed inside the condensation chamber, where the temperature is approximately 1300 K [16]. At these temperatures the figures given above do not hold. Furthermore it is not known [16] exactly what happens inside the condensation chamber, and it is outside the scope of this project to explain it. We will therefore not be dealing with this part of the particle production process.

The time in which the particle stays inside the condensation chamber, accounts for about $\frac{1}{4}$ of the time it uses to travel the distance to the sample holder [16]. The total length from the cathode to the sample holder is approximately 20 cm.

In table 8 we have calculated the average number of collisions with O_2-molecules for an iron oxide particle on its way from the nozzle to the sample holder. The detailed calculations are presented in appendix A. A particle with radius 5 nm contains $\sim 10^5$ atoms. The number of

Radius of particle nm	0.2 % # collisions	0.02 % # collisions
2.5	$5{\cdot}10^4$	$5{\cdot}10^3$
5.0	$2{\cdot}10^5$	$2{\cdot}10^4$
25	$5{\cdot}10^7$	$5{\cdot}10^6$

Table 8: *Calculated number of collisions in the second chamber in the HCCS, for selected particle sizes.*

collisions is thus comparable to the number of atoms in the particle.

8.6 Particle Model

Let us assume that the iron oxides formed in the condensation chamber are wüstite.

In flight the iron oxide particles hit O_2-molecules, and become oxidised on the surface of magnetite (Fe_3O_4), which forms a shell protecting the wüstite in the centre of the particle. The Caberra-Mott oxidisation model and the results on particle composition obtained from Mössbauer spectroscopy, indicate that a possible structure of the iron oxides particles is (illustrated in figure 17):

1. A pure stoichiometric wüstite (FeO) core. In the samples containing pure iron (Fe), there may be a core of iron, surrounded by stoichiometric wüstite (FeO).
2. Around the core, there is a layer of non-stoichiometric wüstite ($Fe_{1-x}O$).
3. At the surface of the particle there is a layer of magnetite (Fe_3O_4) protecting the inner layers from oxidisation.

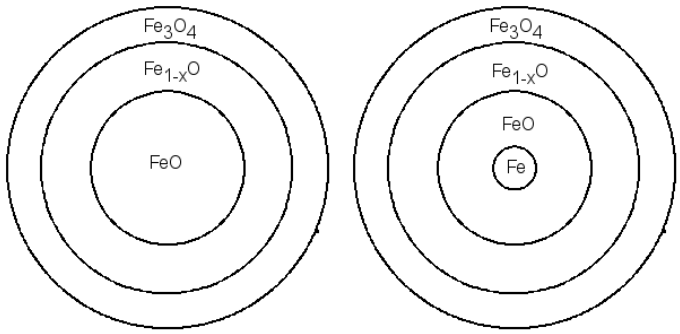

Figure 17: Left: *Schematic of the proposed composition of particles containing only wüstite, and magnetite (Fe_3O_4).* Right: *Schematic of the proposed composition of particles containing wüstite, magnetite (Fe_3O_4) and iron (Fe). The scaling of the schematics is not true.*

It must be emphasised, that this is only a possible explanation, and that the structure could be entirely different. The force of the model is however, that it does explain how the samples still contain wüstite after exposure to air for several weeks.

This provides us with a method of estimating the particle size. According to Caberra-Mott, the oxide layer on the particles is 2.67 nm after 3 weeks of exposure to air. This is found from solving (8.3) numerically. From Mössbauer spectroscopy we find that magnetite (Fe_3O_4) constitutes approximately 50 % of the particles. With this knowledge, and our particle model in mind, we can calculate an estimate of the mean particle diameter to be ∼26 nm. The calculations are presented in Appendix B.

A few days prior to the deadline of the project we obtained some images of particles, produced during a 0.02 % O_2 run, taken with SEM[8]. These images indicate that our particle model is correct, as the size of the particles on the images, corresponds well with our estimate. The resolution of the SEM is approximately 5 nm [17]. The SEM images are presented in figure 18.

We have made some statistics on the particle sizes in the SEM images. These are presented in figure 19. The mean particle diameter from these observations is $\bar{d}$ =26±2 nm. This is in accordance with the particle model.

8.7 The iron spectrum versus the particle model

Our model does not explain why we do not see any magnetite (Fe_3O_4) or other higher oxidised iron oxides, in the JK010 sample. As earlier mentioned, iron is very easily oxidised, so there should be a shell of magnetite. The reason could be as follows:

Iron is a strong ferromagnet. The Mössbauer spectrum shows both superparamagnetic and ferromagnetic iron. We assume that the particles are singledomains (d<100 nm) [16].

The small iron particles are superparamagnetic, and the thin magnetite (Fe_3O_4) layer is far from thick enough to be in another domain. Although the iron is seen as superparamagnetic, it still has a total dipole moment. As earlier mentioned detection of superparamagnetism depends on observation time. The magnetic field from the dipole will dominate the magnetite layer, causing

[8] Scanning Electron Microscope.

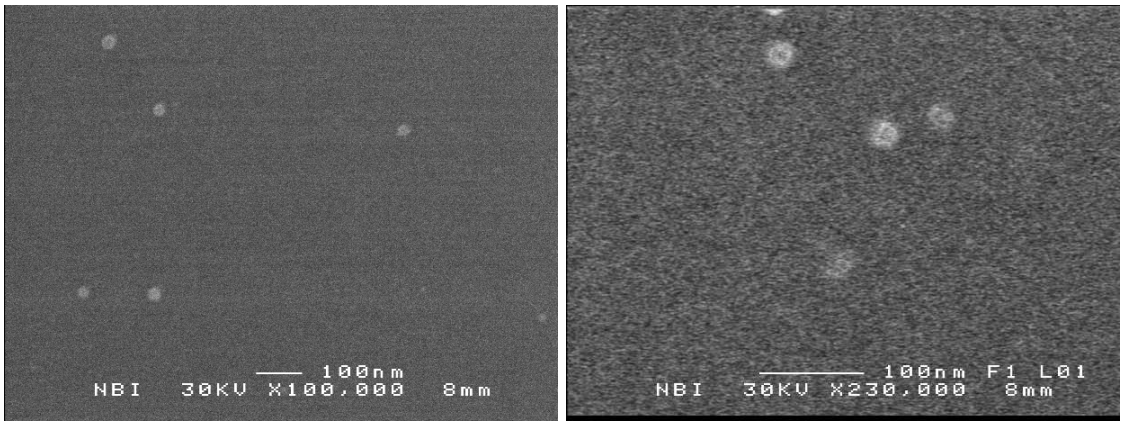

Figure 18: Left: *SEM image of particles produced during JK011 sputtering run. The magnification is 100,000.* Right: *SEM image of particles produced during JK011 sputtering run. The magnification is 230,000. SEM images by Claus B. Sørensen.*

Particle # #	Measured diameter nm
1	29
2	27
3	23
4	18
5	31
6	31
7	31
8	28
9	14

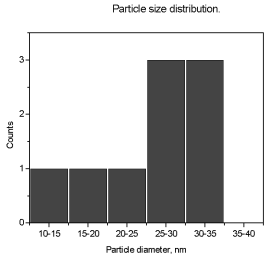

Figure 19: *Rough particle size distribution, calculated from images shown in figure 18.*

it to fluctuate along with the dipole. This will cause magnetite to be seen as a doublet in a Mössbauer spectrum.

The larger ferromagnetic iron particles also have a thin magnetite layer. The magnetic field of the ferromagnetic iron core, forces the dipole moments of the mangetite to align with the magnetic field of the ferromagnet. This interaction causes destruction of the usual magnetic structure of magnetite, and thereby of the spectral lines.

It is therefore likely that the component earlier fitted with non-stoichiometric wüstite ($Fe_{1-x}O$) is magnetite on the iron particles. An isomer shift of 0.817 mm/s is relatively close to 0.67 mm/s, especially when we are analysing a noisy spectrum (see figure 13), and since the particles are very small.

9 Conclusion

In the following section we will try to make some conclusions regarding the topics treated in this project. We will make conclusions for each topic separate.

9.1 Sputtering

Our objective in sputtering, was to examine if it is possible to produce iron oxides via sputtering, using an oxygen (O_2) and argon (Ar) gas mixture. We have found two gas mixtures for which sputtering is possible: 0.2 % and 0.02 % O_2. Of these the 0.02 % O_2 is by far the better, due to:

1. By using this gas mixture sputtering is possible at low currents and lower pressure, making the cathode last longer, thereby making particle production possible for a longer time span.

2. The particle production is easy to stabilise.

3. Using this gas mixture it is to a great extent possible to control the particle deposition rate. This makes it possible to a certain extent, to control the particle size [16].

We have with the 0.02 % O_2 gas mixture, found a suitable gas mixture for sputtering using oxygen in the sputtering gas.

As mentioned we failed in our original objective to produce nano-sized Fe_2O_3. If future attempts are made to produce hematite (α-Fe_2O_3) or maghemite (γ-Fe_2O_3), we recommend to try using gas mixtures with 0.05 % to 0.1 % O_2 with low deposition rates. This should increase the oxidisation power of the gas. These gas mixtures should on the other hand contain sufficiently little O_2, to make stabilisation of the sputter source possible, at low currents (and thus low temperatures) and pressure.

Furthermore we strongly recommend a method of measuring the temperature of the plasma inside the HCCS. The roughly estimated temperature of 1300 K is relatively close to the temperature above which hematite and maghemite are unstable. If the temperature of the plasma is found to be above 1700 K, it is impossible to produce either hematite or maghemite using the sputter source.

9.2 Mössbauer and wüstite

We have produced stable wüstite, stoichiometric (FeO) and non-stoichiometric ($Fe_{1-x}O$). We have examined these particles using Mössbauer spectroscopy, and the parameters found are listed in table 9. These data correspond very well with values found in the literature (see table 4). Especially the values for stoichiometric wüstite (FeO) are good, and show very little variation. The values for non-stoichiometric wüstite ($Fe_{1-x}O$) show a greater variation, but this is not unexpected, since the x is variable between 0 and 0.15.

We have proposed a model (see section 8.6) which explains how the wüstite is stabilised, by a protective shell of magnetite. Based on the model we have estimated a particle size which is confirmed by SEM images.

Component name	0.2 % O_2		0.02 % O_2	
	δ mm/s	E_Q mm/s	δ mm/s	E_Q mm/s
Stoichiometric wüstite, FeO	1.039	0.354	1.036	0.432
Non-stoichiometric wüstite, $Fe_{1-x}O$	0.790	0.828	0.960	0.730

Table 9: *Found Mössbauerparameters for wüstite at room temperature.*

During the writing process we have not been able to find literature on Mössbauer spectroscopic results on wüstite at low temperatures. This could indicate that these data are not known. We have strongly indicated that wüstite is not destroyed by cooling to 17 K, and thereafter heated back to 295 K. With these results we have shown that wüstite can be studied using Mössbauer spectroscopy at low temperatures, thereby making a contribution of unknown data to science.

We strongly encourage the future study of low temperature wüstite, made possible with this discovery.

9.3 A final word

Looking back on the work presented we feel a little uneasy. There are so many loose ends and unsolved problems which could have been pursued.

The fact that no maghemite (γ-Fe_2O_3) and no hematite (α-Fe_2O_3) were produced certainly points to the fact, that in gas-solid reactions these highly oxidised iron compounds are not so easily produced.

Has the results presented any relation to the study of the Martian surface? Was the surface of Mars oxidised via gas-solid reactions during 4 billion years or did liquid water play the essential role? We do not think that any conclusion regarding Mars can be made from the obtained results.

Much more work on the oxidation of the small iron particles has to be done before we can make any profound conclusion concerning oxidation via gas-solid reactions.

A Mean Free Path

We will give an estimate of how much the particles are oxidised from the time of leaving the plasma, until they reach the sample holder. The ideal gas equation is

$$PV = NRT, \tag{A.1}$$

where P is pressure, V is the volume, N the number of gas molecules, R is the gas constant and T is temperature.

The particles travel at a near supersonic speed, and the conditions for the validity of the ideal gas equation are therefore not entirely fulfilled. We will however proceed with the calculations assuming that the system behaves as a ideal gas. Due to the mentioned conditions the following calculations are not entirely accurate.

The pressure is $3.2{\cdot}10^{-2}$ Torr$\simeq$4.27Pa. The partial pressure of oxygen in the two concentrations used is: $P_{0.2\,\%\,O_2}$=$8.5{\cdot}10^{-3}$ Pa, $P_{0.02\,\%\,O_2}$=$8.5{\cdot}10^{-4}$ Pa.

From [25] we get the following expression for the mean free path for a O_2 molecule in a O_2-gas:

$$l = \frac{1}{n\sigma} \quad \text{where} \quad n = \pi r^2, \tag{A.2}$$

where n is the number of molecules per volume, r is the radius of the gas molecule (which for O_2 is r_{O_2} =1.80 Å. [25])[9].

For a particle much larger than a molecule we have to multiply (A.2) by a factor C:

$$C = \frac{A_{\text{particle}}}{A_{O_2-\text{molecule}}} = \frac{r^2_{\text{particle}}}{r^2_{O_2}}, \tag{A.3}$$

where A_{particle} it the cross section area of the iron oxide particle, and $A_{O_2-\text{molecule}}$ is the cross section area of a O_2-molecule. Using the ideal gas equation (A.1), the mean free path (A.2), and assuming that the particle behaves as C O_2-molecules travelling parallel with the same velocity, we obtain the equation

$$l = \frac{1}{\frac{RT}{P}\pi r^2_{O_2} C} \Longrightarrow \tag{A.4}$$

$$N_{\text{collisions}} = \frac{L}{l}, \tag{A.5}$$

If inserted into this last equation one get the number of O_2molecules that a iron oxide particle encounters on its way to the sample holder.

B Calculation of particle size

From Caberra-Mott model of oxidation we have that the oxide layer after 3 weeks is 2.67 nm, and is growing very slowly. From Mössbauer spectroscopy we know that magnetite is about 50 % of the total particle material. The particles are assumed to have spherical shape. The volume and

[9] Assuming that it is shaped as a sphere

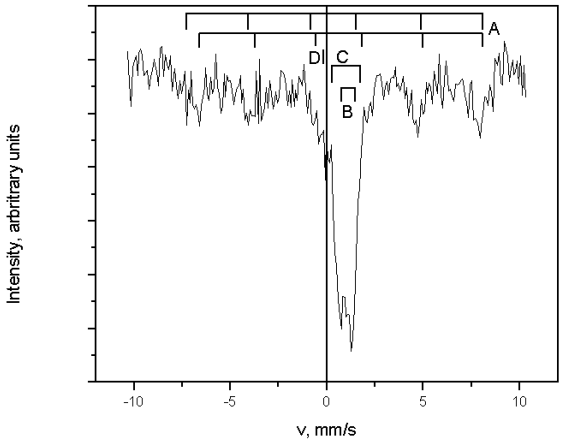

Figure 20: *Control measurement of the JK003, after it has been subjected to cooling to 17K, and thereafter heated to 295 K. The fitted spectra are indicated.*

radius of the particle are related as $V = \frac{4}{3}\pi r^2 \Rightarrow V \propto r^3$. We can set up the following relations for the particle (ignoring the factor $\frac{4}{3}\pi$):

$$2V_{\text{core}} = V_{\text{particle}} \tag{B.1}$$

$$V_{\text{particle}} = 2r^3_{\text{core}} = r^3_{\text{particle}} \tag{B.2}$$

$$r_{\text{particle}} = \sqrt[3]{2} r_{\text{core}} \tag{B.3}$$

$$r_{\text{particle}} = r_{\text{core}} + r_{\text{layer}} \tag{B.4}$$

$$\frac{r_{\text{particle}}}{r_{\text{core}}} = 1 + \frac{r_{\text{layer}}}{r_{\text{core}}} = \sqrt[3]{2} \Rightarrow \tag{B.5}$$

$$r_{\text{core}} = \frac{r_{\text{layer}}}{\sqrt[3]{2} - 1}. \tag{B.6}$$

By inserting the known magnetite layer thickness (2.67 nm) into (B.6), the core (wüstite) diameter is found to be 10.3 nm, and the diameter of the particle thus to be approximately 26 nm.

C Control measurement of wüstite

D Mössbauer constants

Values are from Mørup [21].

Mean life time for ^{57}Fe(I=$\frac{3}{2}$)	$\tau_{\frac{3}{2}}$	$141.1 \cdot 10^{-9}$ s.
g-factor, excited state	g_e	-0.10355.
g-factor, ground state	g_g	-0.181208.
Quadrupole moment, ground state	Q_g	$0\,\text{m}^2$.
Quadrupole moment, excited state	Q_e	$0.21 \cdot 10^{-28}\,\text{m}^2$.
Cross section for resonant absorption	σ_0	$2.57 \cdot 10^{-22}\,\text{m}^2$.

E Selected mineral properties

Lattice constant for wüstite, $Fe_{0.935}O$ [18, p.4-155]	a	4.3088Å.

F Experimental data for the sputter source

Our experimental data for the sputter source are listed the tables in the following sections. The listed data is obtained during the manufacturing of the samples analysed in the report.

The time, t, is listed in minutes as the experiment proceeds. The pressure, P, is measured in the condensation chamber. The pressure is measured in unit of Torr, where 1 Torr equals 1.33 hPa. U_{cat} is the voltage on the cathode and is measured in volts. I_{cat} is current from the cathode through the plasma to the anode measured in amperes. l-U is our controlled ground voltage for the anode measured in volts. Remarks are our comments during the experiment.

F.1 JK003

Experiment *JK003*. Conducted 22.02.01 from 14.00 to 06.00 with 0.2% O_2 and Ar gas-mixture. The experiment was made in two runs due to a overloaded quartz-crystal. The runs are listed in tables 10 and 11.

t min	P Torr	U_{cat} V	I_{cat} A	l-U A	Remarks
0	1.0	321	0.100	4.7	Heating...
17	1.0	328	0.200	4.7	
33	1.0	342	0.300	4.7	
48	1.0	345	0.400	4.7	
64	1.0	347	0.450	4.7	
85	1.0	348	0.500	4.7	
103	1.1	350	0.550	4.7	Sparking.
121	1.1	353	0.600	4.7	Again some sparking.
125	-	-	-	-	Increasing pressure slowly.
126	1.2	355	0.600	4.7	Some sparking.
131	1.3	356	0.600	4.7	Some adjustment of pressure and I_{cat}
-	-	-	-	-	Trying to get a beam by varying pressure and current.
161	2.2	371	0.698	4.7	Turned the sample holder towards the beam. dep$\in$ [1.6; 1.7] Å/sec.
194	-	-	-	-	There was no beam. I_{cat}=0.600 A, increased pressure. No beam. P=1.0 Torr, varying the current up and down.
239	2.2	376	0.855	4.7	dep=0.4 Å/sec. Turned the sample holder towards the beam.
308	2.2	377	0.855	4.7	dep=0.5 Å/sec. Adjusted the position of the cathode to 10.2 cm in search of dep.
394	2.0	378	0.700	4.7	dep=0.9 Å/sec. Stable after sparking.
454	2.0	379	0.640	4.7	dep=0.9 Å/sec.
481	-	-	-	-	The experiment stopped because the quartz crystal was overloaded.

Table 10: *Table of the experimental data of the first run, manufacturing JK003 with a 0.2% O_2 and Ar gas-mixture.*

t min	P Torr	U_{cat} V	I_{cat} A	l-U A	Remarks
0	0.99	339	0.100	4.7	Heating...
16	1.0	344	0.200	4.7	
31	1.0	348	0.300	4.7	
46	1.0	350	0.401	4.7	
63	1.0	351	0.450	4.7	
78	1.0	352	0.500	4.7	Some sparking
95	1.0	354	0.550	4.7	
113	1.0	354	0.600	4.7	
130	1.2	355	0.650	4.7	
145	1.9	370	0.650	4.7	dep$\in$ [1.5; 1.6] Å/sec. Turned the sample holder toward the beam.
170	-	-	-	-	dep=0.4 Å/sec
175	1.9	373	0.700	4.7	dep$\in$ [1.2; 1.3] Å/sec
197	1.9	374	0.754	4.7	dep=1.1 Å/sec
210	1.9	374	0.769	4.7	dep=0.8 Å/sec
230	1.9	374	0.769	4.7	dep=0.8 Å/sec
272	2.0	375	0.769	4.7	dep=0.9 Å/sec
335	1.9	375	0.843	4.7	dep=0.5 Å/sec
365	-	-	-	-	The experiment is stopped and the sample is placed in a vacuum chamber.

Table 11: *Table of the experimental data of the second run, manufacturing JK003, with a 0.2% O_2 and Ar gas-mixture.*

t min	P Torr	U_{cat} V	I_{cat} A	I-U A	Remarks
0	1.0	305	0.100	4.7	Heating... t=9 min U_{cat} drifted to 321 V.
10	1.0	327	0.150	4.7	-
30	1.1	326	0.200	4.7	-
46	1.0	326	0.250	4.7	Pressure decreased due to unstable U_{cat}.
73	1.9	336	0.500	4.7	Achieved after adjustments owing to ΔU_{cat}=30 V.
115	-	-	-	-	Has been very unstable, ΔU_{cat}=30 V.
135	1.1	317	0.589	4.7	Stable.
145	-	-	-	-	Trying to stabilise the apparatus. ΔU_{cat}=35 V, sparking.
151	1.1	320±8	0.531	4.7	
265	1.1	332	531	4.7	Periodic U_{cat}=302 V. dep∈ [0.1 : 1.2] Å/sec.
385	1.1	332	531	4.7	Periodic U_{cat}=302 V. dep∈ [0.1; 3.4] Å/sec.
475	1.1	332	531	4.7	Periodic U_{cat}=302 V. dep∈ [0.1 : 1.9] Å/sec. The experiment is stopped.

Table 12: *Table of the experimental data manufacturing JK010 with pure Ar gas.*

F.2 JK010

Experiment *JK010*. Conducted 03.04.01 from 14.35 to 22.30 with pure Argon gas. The run is listed in table 12.

F.3 JK011

Experiment *JK011*. Conducted 06.04.01 from 14.35 to 23.15 with 0.02% O_2 and Ar gas-mixture. The runs are listed in tables 13 and 14.

t min	P Torr	U_{cat} V	I_{cat} A	I-U A	Remarks
0	1.0	321	0.100	4.7	Heating...
17	1.0	328	0.200	4.7	
33	1.0	342	0.300	4.7	
48	1.0	345	0.400	4.7	
64	1.0	347	0.450	4.7	
85	1.0	348	0.500	4.7	
103	1.1	350	0.550	4.7	Sparking.
121	1.1	353	0.600	4.7	Again some sparking.
125	-	-	-	-	Increasing pressure slowly.
126	1.2	355	0.600	4.7	Some sparking.
131	1.3	356	0.600	4.7	After some adjustment of pressure and I_{cat}
-	-	-	-	-	Trying to get a deposition by varying pressure and current.
161	2.2	371	0.698	4.7	Turned the sample holder towards the beam. dep∈ [1.6; 1.7] Å/sec.
194	-	-	-	-	There was no dep. I_{cat}=0.600 A, increased pressure. P=1.0 Torr, varying the current "up and down".
239	2.2	376	0.855	4.7	dep=0.4 Å/sec. Turned the sample holder towards the beam.
308	2.2	377	0.855	4.7	dep=0.5 Å/sec. Adjusted the position of the cathode to 10.2 cm in search of dep.
394	2.0	378	0.700	4.7	dep=0.9 Å/sec. Stable after sparking.
454	2.0	379	0.640	4.7	dep=0.9 Å/sec.
481	-	-	-	-	The experiment stopped because the quartz crystal was overloaded.

Table 13: *Table of the experimental data of the first run, manufacturing JK011 using a 0.02% O_2 and Ar mixture*

t min	P Torr	U_{cat} V	I_{cat} A	l-U A	Remarks
0	1.0	291	0.100	4.7	Heating...
15	1.1	331	0.200	4.7	
30	1.2	333	0.275	4.7	
50	1.3	336	0.350	4.7	
60	1.5	342	0.400	4.7	dep increased from 0.1 Å/sec to 0.7 Å/sec in 10 min
70	1.5	343	0.400	4.7	dep=0.8 Å/sec and increasing
75	1.5	343	0.400	4.7	dep=2.2 Å/sec, target turned towards the beam
85	1.5	343	0.400	4.7	dep=5.5 Å/sec
105	1.5	343	0.400	4.7	dep=12 Å/sec, trying to decrease dep to 5 Å/sec
110	-	-	-	-	Cannot get the apparatus stable
140	-	-	-	-	Decided to run another experiment. New quartz crystal and mounted a Silicium chip to collect particles for SEM.
140	1.0	333	0.150	4.7	
150	1.1	334	0.250	4.7	
160	1.2	338	0.350	4.7	
175	1.4	344	0.400	4.7	dep is increasing
176	-	-	0.380	-	To prevent dep increasing
185	1.4	342	0.350	4.7	dep$\in$[3.2;4.8] Å/sec. Sample holder turned toward beam
260	1.4	343	0.350	4.7	dep$\in$[5.1;6.3] Å/sec
295	1.3	343	0.350	4.7	dep$\in$[4.1;4.9] Å/sec
370	-	-	-	-	Got a big area of material

Table 14: *Table of the experimental data of the second run, manufacturing JK011, with a 0.02% O_2 and Ar gas-mixture.*

References

[1] B. Miczko A. Pattek-Janczyk, J.-C. Grenier. Wustite phase transformation in iron catalysts for ammonia synthesis. *Solid State Ionics*, 117:95–103, 1999.

[2] Canard. Macfit, 1998. Demo Computer Program.

[3] R. S. Carmichael. *Practical handbook of Physical Properties of Rocks and Minerals.* CRC Press, Department of Geology, University of Iowa, 1989.

[4] Sargent-Welch Scientific Company. Periodic table of the elements, 1979.

[5] B. D. Cullity. *Introduction to magnetic materials.* Addison Wesley, 1 edition, 1972.

[6] B. Elbek. *Elektromagnetisme.* Niels Bohr Institutet, 1997.

[7] D. J. Griffiths. *Introduction to Electrodynamics.* Prentice-Hall, 3 edition, 1999.

[8] M.F. Hansen. Super-para-magnetisme i mars-støv-analogier. Master's thesis, HCØ, NBI, KU, August 1995.

[9] K. O. Christensen J. íHjøllum. Spmtoexp konverter. Computer programme for conversion of spm-files to exp-files, Marts 2001. www.geocities.com/jarihj/software/konv.zip.

[10] C.S. Lee J.C. Park, D. Kim and D.K. Kim. A new synthetic route to wüstite. *Bull. Korean Chem. Soc.*, 20(9), 1999.

[11] M. B. Madsen J.M. Knudsen. Magnetic properties experiment on mars pathfinder. Technical report, NBI, KU, 1995.

[12] S. Wissman K.D. Becker, D. Niemeier, M. Oversluizen, J.W. Couves, and A.V. Chadwick. A high-temperature xafs study of iron oxides. *Nuclear Instruments and Methods in Physics Research*, B 97:111–114, 1994.

[13] C. Kittel. *Introduction to Solid State Physics.* John Wiley & Sons, Inc., 7 edition, 1996.

[14] C. Kittel and J. K. Galt. Ferromagnetic domain theory. *Solid State Physics*, 3:437–564, 1956.

[15] J. M. Knudsen. Discussion and conversation with J. M. Knudsen April 2001.

[16] L. T. Kuhn. Discussion and conversation with L. T. Kuhn about sputtering, and the hollow cathode sputtering machine, Jan-Apr 2001.

[17] L. T. Kuhn. *Studies of isolated single crystalline nanoparticles by a ballistic Hall micromagnometer.* PhD thesis, Ørsted Laboratory, NBIfAFG, KU, December 1998.

[18] D. R. Lide. *Handbook of Chemistry and Physics*, volume 79. CRC Press, 1998-1999 edition, 1998. The Rubber Bible.

[19] M. B. Madsen. Discussion and conversation with M. B. Madsen, Jan-Apr 2001.

[20] H.P. Gunnlaugsson M.B. Madsen, S.F. Hviid, J.M. Knudsen, W. Goetz, C.T. Pedersen, A.R. Dinesen, C.T. Mogensen, and M. Olsen. The magnetic properties expriments on mars pathfinder. *Journal of Geophysical research*, 104(E4):8761–8779, April 1999.

[21] S. Mørup. *Mössbauerspectroscopy and its applications in materials science.* Physics dep. DTU, 1994.

[22] I.V. Murin, V.M. Smirnov, G.P. Voronkov, V.G. Semenov, V.G. Povarov, and B.M. Sinel'nikov. Structural-chemical transformations of α-Fe_2O_3upon transport reduction. *Solid State Ionics*, 133:203–210, 2000.

[23] M. D. Bentzon S. Linderroth, S. Mørup. Oxidation of nanometer-sized iron particles. *Journal of Materials Science*, 30:3142–3148, 1995.

[24] B. S. Clausen S. Mørup, H. Topsøe. Magnetic propertie of microcrystal studied by Mössbauerspectroscopy. *Physica Scripta*, 25:713–719, 1982.

[25] Sears & Sallinger. *Thermodynamics, Kinetic Theory, and Statistical Thermodynamics.* Addison Wesley, 3 edition, 1986.

[26] V. W. A. Vieira. *The oxidation state of iron in the early solar system.* PhD thesis, H. C. Ørsted Institute, University of Copenhagen, June 1985.

[27] T. Miyano Y. Sakisaka and M. Onchi. Electron-energy-loss-spectroscopy study of oxygen chemisorption an initial of fe(100). *Physical Review B*, 30(12):6849, 1984.